

Targeted mixing in an array of alternating vorticesR. Bachelard,¹ T. Benzekri,^{1,2} C. Chandre,¹ X. Leoncini,^{1,3} and M. Vittot¹¹*Centre de Physique Théorique, CNRS Aix-Marseille Universités, campus de Luminy, Case 907, F-13288 Marseille cedex 9, France*²*Université des Sciences et de Technologie HB, BP 32 EL Alia, Bab Ezzouar Alger, Algeria*³*PIIM, Université de Provence-CNRS, Centre Universitaire de Saint Jérôme, F-13397 Marseille, France*

(Received 16 July 2007; published 19 October 2007)

Transport and mixing properties of passive particles advected by an array of vortices are investigated. Starting from the integrable case, it is shown that a special class of perturbations allows one to preserve separatrices which act as effective transport barriers, while triggering chaotic advection. In this setting, mixing within the two dynamical barriers is enhanced while long range transport is prevented. A numerical analysis of mixing properties depending on parameter values is performed; regions for which optimal mixing is achieved are proposed. Robustness of the targeted mixing properties regarding errors in the applied perturbation are considered, as well as slip/no-slip and/or boundary conditions for the flow.

DOI: [10.1103/PhysRevE.76.046217](https://doi.org/10.1103/PhysRevE.76.046217)

PACS number(s): 05.45.Gg, 47.52.+j, 47.51.+a

I. INTRODUCTION

Since its uncovering, chaotic advection [1,2] has drawn much attention as its consequences on both transport and mixing properties of a given flow are fundamental. This phenomenon is closely related to Lagrangian chaos, and translates the fact that despite the laminar character of the flow Lagrangian, trajectories of a fluid or passive particles may end up being chaotic. In this setting, transport and mixing properties are drastically changed [3–6]. In chaotic regions of the flow, mixing induced by molecular diffusion becomes often negligible in regards to the mixing induced by the dynamics. Regarding transport properties, the triggering of chaotic advection also plays a key role. Indeed, in contrast to the fully predictive integrable situation, tackling transport properties of individual passive particles is subject to sensitivity to initial conditions and implies a necessary probabilistic approach. This leads in some cases to a diffusion equation with an enhanced diffusion coefficient when compared to the molecular diffusion one [7], but also to non-Gaussian properties of transport (see [8,9]), as for instance, superdiffusive transport. One then often resorts to modeling transport using a fractional diffusion equation [10]. All these properties have drawn much attention not only for its impact on geophysical flows and magnetized plasmas [9,11–18], but also because of the potential applications of its enhanced mixing properties in chemical engineering and microfluidic devices [19,20].

Lagrangian chaos in two-dimensional incompressible flows is triggered generically when the flow becomes time dependent [2,21–24]. The trajectories of fluid particles or passive tracers are not confined on field lines and chaos appears. For these type of flows the dynamics of fluid particles is Hamiltonian, with the stream function acting as the Hamiltonian. The canonically conjugate variables are the space variables, and the phase space is the two-dimensional physical space. This particularity allows direct visualization of phase space in experiments, making it a test bed used to confront theoretical results on Hamiltonian dynamics with experiments. More specifically, passive tracer dynamics belong to the class of Hamiltonian systems with 1.5 degrees of freedom. General mixing and transport properties of these

systems are now well understood, especially when the time dependence is periodic and Poincaré maps are computed to analyze phase space topology. Typically the dynamics is not ergodic: A chaotic sea surrounds various islands of quasiperiodic dynamics. The anomalous transport properties and their multifractal nature are then linked to the existence of islands and the phenomenon of stickiness observed around them [25,26], while mixing is enhanced in the chaotic sea but must rely on molecular diffusion in regular regions.

In most studies regarding this type of phenomena, the time-dependent perturbation is given *a priori* or self-generated. Transport and mixing properties are thoroughly investigated and general laws are extrapolated or the origin of phenomena explained (see [26–29]). The influence of phase space topology and its understanding is clear, and can be used to explain synchronization phenomena [30]. However one is still somewhat constrained by an *a priori* imposed time dependence. Recently, approaches of tailoring specific perturbations in order to modify phase space have been proposed [31,32] and a specific one has been applied to an array of alternating vortices [33]. Due to the strong influence of invariant tori forming regular islands on global transport and mixing properties, acting on phase space topology even locally (for instance, by building a transport barrier [31,33] or by destroying regular islands [33]) can have strong consequences.

In this paper we address the problem of targeted mixing, a work already started in Ref. [33]. We refer to targeted mixing as the process of leveraging only one of the consequences of chaotic advection, namely enhancing mixing, while containing particle transport within a finite subdomain of phase space. For this purpose we consider the dynamics of passive particles in an array of alternating vortices and tailor phase space in order to achieve the desired property. From the experimental point of view, acting on phase space is often not easy, because one must act also on particle momenta in general. However, this may be less of a problem in the context of two-dimensional incompressible flows due to the duality between physical space and phase space. Moreover mixing within flows has a tremendous number of applications. The primary interest in the flow of an array of alternating vortices resides in the fact that being generated by quite a few hydro-

dynamic instabilities, it may be considered as one of the founding bricks of turbulence. This flow is easily accessible to experimentalists, for instance, using magnetohydrodynamics techniques similar to Rayleigh-Bénard convection with a control over the flow [21–23]. As such, understanding its influence on the advection of passive or active quantities is considered a necessary first step in order to uncover the different mechanisms governing transport in general or reaction-diffusion processes such as front propagation in turbulent flows [34–38]. The stream function which models an experiment in a channel with slip boundary conditions is

$$\Psi_0(x,y) = \sin x \sin y, \tag{1}$$

where the x direction is the horizontal one along the channel and the y direction is the bounded vertical one. The dynamics given by the stream function (1) is integrable and passive particles follow the stream lines, no mixing occurs. In the experiments, a typical perturbation $f(x,y,t)$ is introduced as a time-dependent forcing in order to trigger chaotic advection and then to study the resulting transport and mixing properties. More precisely we consider perturbations which modify the stream function as

$$\Psi_c(x,y,t) = \Psi_0(x+f,y). \tag{2}$$

We show how to identify the perturbations f which preserve transport barriers and at the same time, enhance mixing properties.

The paper is organized as follows: In Sec. II we recall some basic notions of passive scalar dynamics in two-dimensional incompressible flows. Then we give a short review of possible Hamiltonian control techniques we use in order to tailor a perturbation best suited for our needs. In Sec. III, we apply these techniques to flows modeled by the stream function (1). First we derive the perturbation needed in order to build virtual barriers along the channel and thus limit transport within only a small region of phase space. Then among all possible perturbations, we define criteria needed to achieve good mixing within the two barriers and analyze for which perturbations and parameters these criteria are satisfied. Then, we consider the robustness of the proposed perturbation with respect to a simpler time dependence, slip boundary conditions, three-dimensional effects and molecular diffusivity. After showing the efficiency of such perturbations in enhancing mixing, we analyze the set of parameters for which efficient mixing is expected using the residue method.

II. A STRATEGY FOR MIXING INSIDE A CELL

The term advection by definition, relates to the action of being moved by and with a flow. In mathematical terms, this translates in the general equation for a passive tracer,

$$\dot{\mathbf{r}} = \mathbf{v}(\mathbf{r},t), \tag{3}$$

where \mathbf{r} locates the passive tracer in space, \mathbf{v} corresponds to the velocity field, and $\dot{\mathbf{r}}$ corresponds to the time derivative of \mathbf{r} . In the case of two-dimensional incompressible flows, the study of the field can be described by a scalar function, i.e.,

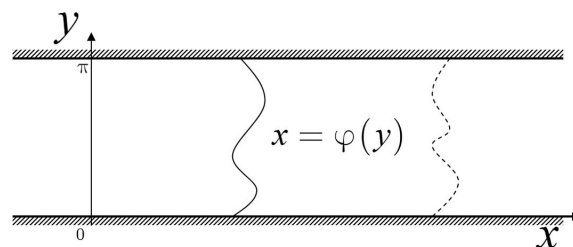


FIG. 1. Schematic representation of the channel with a transport barrier located at $x=\varphi(y)$.

the stream function $\psi(\mathbf{r},t)$. The velocity field is then obtained by $\mathbf{v}=\text{curl}(\psi\hat{\mathbf{z}})$, where $\hat{\mathbf{z}}$ is the unit vector normal to the flow. Equation (3) is rewritten using the stream function and exhibits a Hamiltonian structure for the flow,

$$\dot{x} = -\frac{\partial\Psi}{\partial y}, \quad \dot{y} = \frac{\partial\Psi}{\partial x}, \tag{4}$$

where (x,y) corresponds to the coordinates of the tracer on the plane. The space variables (x,y) are canonically conjugate for the stream function Ψ which acts as the Hamiltonian of the system. Hence, the phase space is formally the two-dimensional physical space (with the addition of time).

In this section, our aim is to briefly recall some Hamiltonian techniques allowing to some extent, to tailor phase space by adjusting appropriately the perturbation f as in Eq. (2) and its parameters. These techniques will be subsequently used to achieve targeted mixing for the considered flows, namely construct a perturbation in order to obtain optimal chaotic mixing in a localized region of phase space. First we construct a family of perturbations which create transport barriers, then we use the residue method [32] in order to find optimal mixing regimes in parameter space after the barriers have been created.

A. Constructing a perturbation with a barrier

We consider a generic time-independent stream function (Hamiltonian) $\Psi_0(x,y)$ describing a fluid in a two-dimensional channel of height π , i.e., $(x,y) \in \mathbb{R} \times [0, \pi]$ (see Fig. 1). We assume that there exists an invariant curve which prevents the advection of tracers from the left to the right of that curve. We denote the equation of this curve $x=\varphi(y)$. The invariance condition $[\dot{x}=\varphi'(y)\dot{y}$ if $x=\varphi(y)]$ of tracers on this curve translates into

$$\Psi_0[\varphi(y),y] = \text{const},$$

for all $y \in [0, \pi]$ by using Eqs. (4). In the case of Eq. (1), this transport barrier is a heteroclinic connection between two hyperbolic fixed points located at $y=0$ and $y=\pi$.

In order to enhance mixing, the system is perturbed by a time-dependent forcing (depending also on x and y in general). As a consequence, its dynamics is generically no longer integrable, and chaotic trajectories fills portions of the channel (these are parts where mixing occurs). However, as a side effect, the transport barrier is broken and trajectories

start to diffuse along the channel (in the x direction).

In the following, we propose to design a time-dependent forcing of the flow described by Ψ_0 which preserves the transport barrier as well as the chaotic mixing. The aim is to find an appropriate forcing which preserves a bounded domain of the channel with an enhanced chaotic mixing inside. This domain can be bounded by two dynamical barriers as mentioned above.

A main practical requirement is that the forcing should be as simple as possible to be implemented. Consequently, we start by investigating perturbations which only depends on y and t . Furthermore, for practical reasons, we restrict the perturbations to time-periodic ones, and the period is chosen as 2π without loss of generality. More precisely, we search for a perturbation $f(y,t)$ which modifies the stream function Ψ_0 into

$$\Psi_c(x,y,t) = \Psi_0[x+f(y,t),y]. \quad (5)$$

In order to simplify the computations, we perform a generic translation in x (which corresponds to a canonical transformation in the Hamiltonian setting),

$$\tilde{x} = x + \partial_y \beta(y,t),$$

$$\tilde{y} = y,$$

where β is a function to be specified later. In the new variables \tilde{x} and \tilde{y} , the dynamics is described by the stream function

$$\tilde{\Psi}_c(\tilde{x},\tilde{y},t) = \Psi_0[\tilde{x}+f(\tilde{y},t) - \partial_y \beta(\tilde{y},t),\tilde{y}] - \partial_t \beta(\tilde{y},t).$$

In order to have an invariant curve acting as a barrier in the channel, the perturbation f is such that the stream function evaluated at $\tilde{x}=\varphi(\tilde{y})$ is only a function of time, since the barrier is time independent (in the moving frame). For simplicity, we consider solutions for which the stream function vanishes,

$$\Psi_0[\varphi(y) + f(y,t) - \partial_y \beta(y,t),y] - \partial_t \beta(y,t) = 0, \quad (6)$$

which is a single equation with two unknown functions, β and f . In principle, there are an infinite set of solutions. Depending on other requirements, some solutions are more appropriate than others. In the following, we choose

$$f(y,t) + \varphi(y) - \partial_y \beta(y,t) = \Phi(t),$$

where $\Phi(t)$ is any function of t . Equation (6) implies

$$\partial_t \beta(y,t) = \Psi_0[\Phi(t),y].$$

This equation has solutions provided that the mean value of $\Psi_0[\Phi(t),y]$ with respect to time vanishes for all y . This guides the choice for the function Φ . A possible solution for β is

$$\beta(y,t) = \Gamma \Psi_0[\Phi(t),y],$$

where

$$\Gamma v(y,t) = \sum_{k \neq 0} \frac{v_k(y)}{ik} e^{ikt},$$

for $v = \sum_k v_k(y) e^{ikt}$. The perturbation f is given by

$$f(y,t) = \Phi(t) - \varphi(y) + \Gamma \partial_y \Psi_0[\Phi(t),y]. \quad (7)$$

The stream function Ψ_c given by Eq. (5) has an invariant curve whose equation is

$$x = \varphi(y) - \Gamma \partial_y \Psi_0[\Phi(t),y]. \quad (8)$$

There exist many more solutions f than the one indicated here. These solutions are obtained by using more complex translation functions β . However, they contain a lot more Fourier modes in y , which make them more difficult to implement for the cases we consider in Sec. III. We notice that the perturbation f given by Eq. (7) as well as the equation of the transport barrier (8) are parametrized by a time-periodic function $\Phi(t)$. This function Φ is in general parametrized by essentially two parameters, its frequency and its amplitude. In parameter space, the dynamics characterized by the stream function Ψ_c exhibit drastically different behaviors depending on the values of parameters. In what follows, we use periodic orbits to determine the regions in parameter space where complete mixing inside the transport barriers occurs. This method is briefly explained in the next section.

B. Periodic orbit analysis

The dynamics of the perturbed flow as the one given by the stream function Ψ_c can be investigated by looking at the (linear) stability of specific periodic orbits, using indicators such as the *residue*. In order to ‘‘control’’ the flow, one can monitor the residues by varying the parameters of the system (like the frequency and the amplitude of the forcing), until specific bifurcations occur. In particular, the residue method allows one to predict the break up (or creation) of invariant tori, which entails an enhancement (or reduction) of chaotic mixing.

We consider a Hamiltonian flow with 1.5 degrees of freedom which depends on a set of parameters $\lambda \in \mathbb{R}^m$,

$$\dot{\mathbf{r}} = \mathbb{J} \nabla_{\mathbf{r}} \Psi(\mathbf{r},t;\lambda),$$

where $\mathbf{r}=(x,y)$ and $\mathbb{J}=\begin{pmatrix} 0 & -1 \\ 1 & 0 \end{pmatrix}$. In order to analyze the linear stability properties of the associated periodic orbits, we also consider the Jacobian $J'(\mathbf{r})$ which evolves according to the tangent flow written as [39]

$$\frac{d}{dt} J'(\mathbf{r}) = \mathbb{J} \nabla_{\mathbf{r}}^2 \Psi(\mathbf{r},t;\lambda) J', \quad (9)$$

where J^0 is the two-dimensional identity matrix and $\nabla_{\mathbf{r}}^2 \Psi$ is the Hessian matrix (composed of second derivatives of Ψ with respect to its canonical variables). For a given periodic orbit with period T , the linear stability properties are given by the spectrum of the two-dimensional monodromy matrix J^T . These properties can be synthetically captured in Greene’s definition [40,41] of the residue

$$R = \frac{2 - \text{tr} J^T}{4},$$

since $\det J^T = 1$. In particular, if $R \in]0, 1[$, the periodic orbit is elliptic; if $R < 0$ or $R > 1$ it is hyperbolic; and if $R=0$ and $R=1$, it is parabolic.

The residues of a set of well-selected periodic orbits provide—through linear stability analysis—information to detect the enhancement as well as the reduction of chaotic mixing [32,42]. The actual change of dynamics must be checked *a posteriori* by a nonlinear stability analysis (a Poincaré section for instance). The residues are used to discard regions in parameter space where large elliptic islands are present.

For this purpose, an alternative strategy is to use a “brute force” method and scan a whole range of physically relevant parameters, analyze transport and mixing properties (by a Poincaré map inspection, for instance), and conclude on a domain of parameters where optimal mixing is achieved. Though it would be a complete analysis, this strategy is not reasonable to adopt because of the high number of cases to consider and also the computer time it takes to analyze a single case.

In order to circumvent these difficulties we choose to consider the residue method described in this section and follow in parameter space the stability of a well selected set of periodic orbits. Indeed due to the Hamiltonian nature of passive particles, one can expect a direct correspondence between nonmixing regions in physical space and islands of stability in phase space. The higher the period of the island, the smaller is its size, hence by following the linear stability of elliptic periodic orbits with small period in parameter space, one should be able to define a potential optimal mixing region for which these orbits are unstable and associated with a mixing enhancement. Once this set of main periodic orbits has been defined by close inspection of several situations, the mixing region is obtained by looking at the bifurcation curves in parameter space, e.g., the set of parameters such that the residue is equal to 1 [32]. We will show in the next section how to combine the creation of transport barriers and the residue method in a particular example of stream function given by Eq. (1).

III. ACHIEVING TARGETED MIXING IN AN ARRAY OF VORTICES

The stream function given by Eq. (1) models a cellular flow consisting of alternating vortices. If we restrict ourselves to $y \in [0, \pi]$, we have a channel of alternating vortices with slip boundary conditions. From the Hamiltonian perspective, the advection of passive tracers is given by Eq. (4). Since the flow is steady, trajectories coincide with the fluid streamlines depicted in Fig. 2(a).

Few basic facts explain the structures of the dynamics: Boundary conditions given in $y=0$ and $y=\pi$ constitute invariant curves. The system is 2π periodic in the x direction, i.e., along the channel. The system has hyperbolic fixed points located at $x=m\pi$ for $m \in \mathbb{Z}$ and $y=0$ or $y=\pi$. These points are joined by vertical heteroclinic connections for which the stable and unstable manifolds coincide corresponding to roll boundaries, at the origin of the cellular structure of the flow.

In order to obtain chaotic advection for two-dimensional flows, one must perturb the flow by a time-dependent forcing. For example, one can periodically force the roll patterns

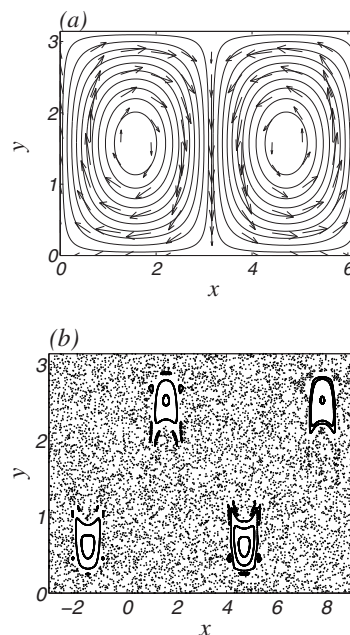


FIG. 2. (a) Streamlines at $t=0$ and (b) Poincaré section of the stream function (10). The parameters are $\omega=1$ and $\epsilon=0.8$.

to oscillate in the x direction [21], in which case the stream function reads

$$\Psi_1(x, y, t) = \sin(x + \epsilon \sin \omega t) \sin y, \quad (10)$$

where $f(x, y, t) = \epsilon \sin \omega t$ acts as a perturbation. The parameter ϵ and ω are, respectively, the amplitude and the angular frequency of these lateral oscillations. The barriers (heteroclinic connections between the hyperbolic periodic orbits) are broken under the perturbation f , which cause the passive particles to undergo chaotic advection along the channel [43].

The streamlines corresponding to the stream function Ψ_1 given by Eq. (10) are depicted in Fig. 2(a). We observe that the structures are essentially the same as those of the stream function Ψ_0 given by Eq. (1). However, the periodic forcing now drives back and forth the roll patterns in the x direction with a period $2\pi/\omega$. The surfaces $y=0$ and $y=\pi$ are left invariant by the perturbation and the hyperbolic orbits persist on these surfaces. The Poincaré section for $\omega=1$ and $\epsilon=0.8$ [see Fig. 2(b)] shows how passive particles are spreading along the channel. Particle transport from roll to roll is greatly enhanced. However, an unmixed area characterized by regular trajectories is still present at the center of each vortex: It is composed of invariant tori of the dynamics. Consequently, though diffusion has appeared in the system due to the time-dependent perturbation, some regular patterns are persistent. Note that increasing the amplitude ϵ does not make them disappear; in particular, in the limit of large ϵ (with ω fixed), the system will be integrable as well.

A. Building transport barriers

In what follows, we propose to adjust the time periodic forcing as explained in Sec. II A. First we notice that

$\Psi_0(m\pi, y) = 0$ for any $y \in [0, \pi]$ and all $m \in \mathbb{Z}$. We apply the construction of the perturbation with $\varphi(y) = 0$ [or equivalently $\varphi(y) = 2m\pi$]. In Eq. (7), we choose $\Phi(t) = \epsilon \sin \omega t$ which gives the perturbation

$$f(y, t) = \epsilon \sin \omega t + \omega^{-1} \cos y C_\epsilon(\omega t), \quad (11)$$

where

$$C_\epsilon(t) = \Gamma \sin(\epsilon \sin t) = -2 \sum_{n \geq 0} \frac{1}{2n+1} \mathcal{J}_{2n+1}(\epsilon) \cos(2n+1)t, \quad (12)$$

and \mathcal{J}_n (for $n \in \mathbb{N}$) are Bessel functions of the first kind. In the numerics, we truncate the sum (12) to five modes. Very similar results are obtained with a higher number of modes.

We notice that since the stream function is still 2π periodic in the x direction by construction, the invariant surface which has been created around $x=0$ is also translated around $2m\pi$, $m \in \mathbb{Z}$. The equations of these transport barriers along the x direction are

$$x = 2m\pi - \omega^{-1} \cos y C_\epsilon(\omega t), \quad (13)$$

for all $m \in \mathbb{Z}$. Notice that these barriers exist for arbitrary values of ω and ϵ . Each of these barriers are heteroclinic connections between two hyperbolic periodic orbits,

$$x(t) = 2m\pi - \omega^{-1} C_\epsilon(\omega t) \quad \text{at } y = 0,$$

$$x(t) = 2m\pi + \omega^{-1} C_\epsilon(\omega t) \quad \text{at } y = \pi,$$

which move in opposite directions. Furthermore, the top and bottom boundaries of the channel remain invariant. This comes from the fact that the perturbation given by Eq. (11) is only applied in the x term of Ψ_0 .

Figure 3(a) depicts the streamlines of the stream function,

$$\Psi_c(x, y, t) = \sin[x + \epsilon \sin \omega t + \omega^{-1} \cos y C_\epsilon(\omega t)] \sin y, \quad (14)$$

at $t=0$ for $\omega=1$ and $\epsilon=0.8$. We notice that the displacement of the rolls remains periodic and parallel to the x direction with an additional oscillating shear. The Poincaré section depicted on Fig. 3(b) reveals the dynamics of tracers which is very different from the one given by the stream function Ψ_1 given by Eq. (10) [see Fig. 2(b)]. The main differences are that barriers suppressing long-range chaotic transport along the channel are restored around $x=0 \pmod{2\pi}$ (bold curves), and that efficient mixing is achieved within the cell confined by two barriers. We observe that passive particles appear to invade the whole confined cell until the fluid is apparently fully mixed; most of the regular trajectories observed for the stream function Ψ_1 are broken by the perturbation.

In Fig. 4, a numerical simulation of the dynamics of a dye of tracers in the fluid is shown. The left-hand column depicts the dynamics of tracers for the stream function (10). The right-hand column shows the mixing of a dye within a cell delimited by two barriers created by the stream function (14). We see that the scattering of the dye, which leads to mixing, occurs through a combination of stretching and folding of the dye in both cases.

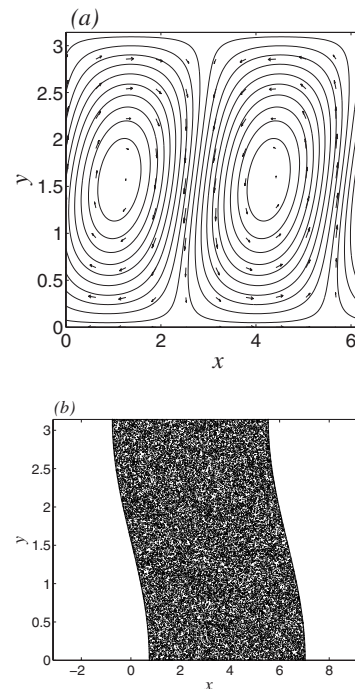


FIG. 3. (a) Streamlines at $t=0$ and (b) Poincaré section of the stream function (14). The parameters are $\omega=1$ and $\epsilon=0.8$.

B. Mixing analysis: Local Lyapunov exponent and mean recurrence time analysis

As the absence of the regular islands from the Poincaré sections does not guarantee the homogeneity of mixing, the study of local properties of mixing in phase space may provide extensive information. For this purpose we consider two different types of analysis, namely the Lyapunov map and the mean recurrence time. Both analysis are performed within the space of initial conditions.

First, in order to get insight into the action of the perturbation on the local stability properties of the system, we compute the Lyapunov map. This method provides local information in phase space. It has been introduced to detect ordered and chaotic trajectories in the set of initial conditions. It associates a finite-time Lyapunov exponent ν with an initial condition (x_0, y_0) at $t=0$. Let us consider the tangent flow (9), and define the maximum finite-time Lyapunov exponent by integrating the flow and the tangent flow over some time τ starting with some initial condition (x_0, y_0) :

$$\nu(x_0, y_0, \tau) = \frac{1}{\tau} \ln |\lambda_{\max}(x_0, y_0, \tau)|,$$

where $\lambda_{\max}(x_0, y_0, \tau)$ is the largest (in norm) eigenvalue of J^τ (one can also use the eigenvalue of $J^{\tau*} J^\tau$ where $J^{\tau*}$ is the transposed matrix of J^τ).

From the inspection of the map $(x_0, y_0) \mapsto \nu(x_0, y_0, \tau)$ for some given time τ , one distinguishes the set of initial conditions leading to regular motion associated with a small finite-time Lyapunov exponent, from the chaotic ones with larger finite-time Lyapunov exponents. Hence, this map reveals the phase space structures where the motion of tracers is trapped

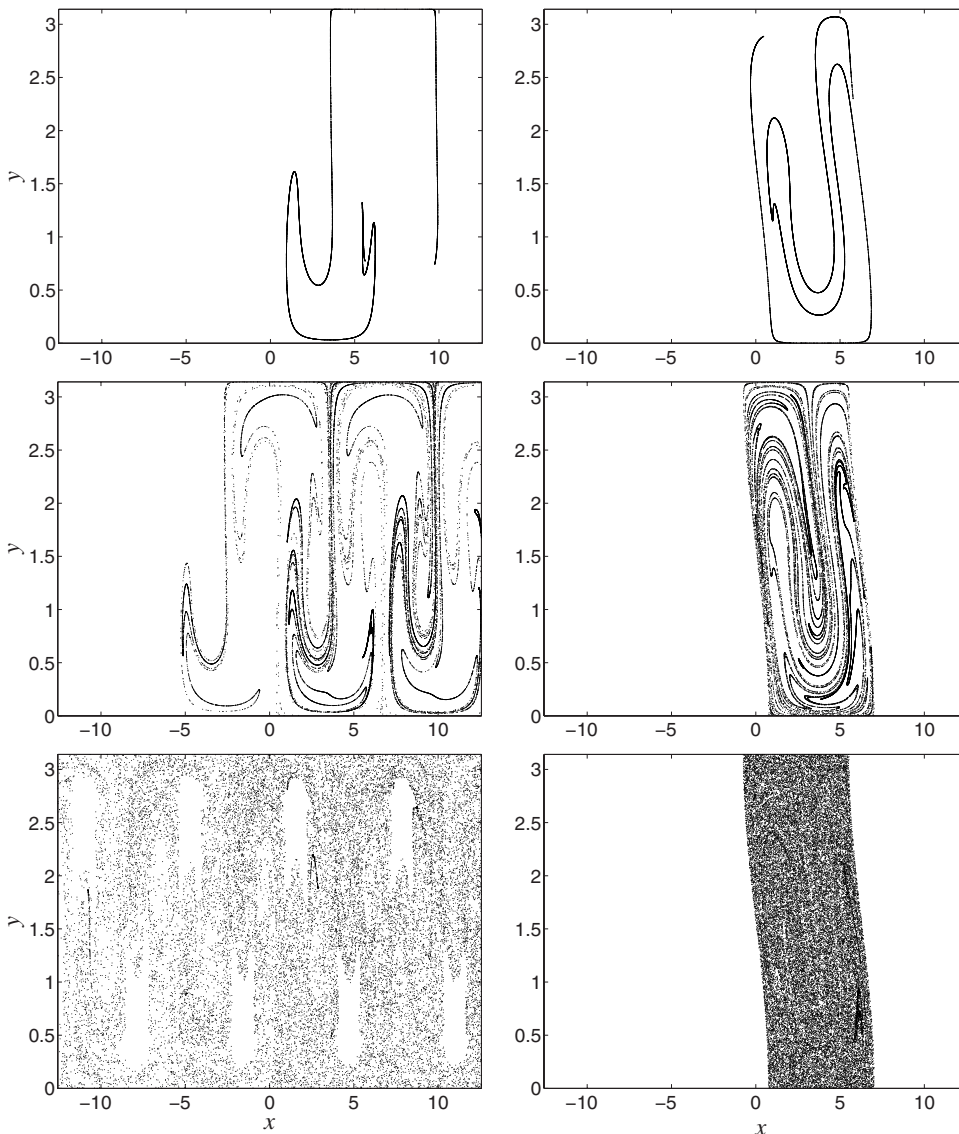


FIG. 4. Numerical simulation of the dynamics of a dye at $t=4T$, $t=6T$, $t=18T$, and $T=2\pi$ (from top to bottom): Left-hand column for the stream function (10) and right-hand column for the stream function (14). The parameters are $\omega=1$ and $\epsilon=0.8$.

on invariant tori, i.e., they highlight islands of stability located around elliptic periodic orbits. Mixing regions are characterized by high values of their finite-time Lyapunov exponents.

Figure 5 represents the Lyapunov maps for the dynamics of tracers given by the stream function (14) for $\omega=1.67$ and $\epsilon=0.63$ (upper panel) and for $\omega=1$ and $\epsilon=0.8$ at a time $T=200\pi$. The dark regions are characteristic of small values of the Lyapunov exponent. We notice that Fig. 5 (upper panel) shows small remaining islands which are barely noticeable in the Poincaré section (see Fig. 3 of Ref. [33]). For mixing studies, the Lyapunov diagnostic seems to be an appropriate tool to reveal small nonmixing regions. These regular regions have disappeared for $\omega=1$ and $\epsilon=0.8$ (lower panel). However, the Lyapunov map is not able to identify the transport barriers which means that locally near the barriers, the motion is as chaotic as inside the cell.

As seen above, by looking at the Lyapunov map, one can infer local mixing properties of the flow. However one can notice that since the created barrier is a separatrix and not a KAM torus as, for instance, in Ref. [31], the existence of the

barrier cannot be detected by the Lyapunov map. To complement this analysis, we consider a second diagnostic namely a recurrence time analysis. An interesting property of return time distributions stems from the fact that they are known to be sensitive both to local and global dynamical properties of phase space. For instance, being in the neighborhood of a hyperbolic periodic orbit versus an elliptic one should affect the distribution [44]. Therefore, the distribution should be affected if computed in the neighborhood of a separatrix, or if trapped within a regular region. Since we have already analyzed the local stability properties of the flow by computing the Lyapunov map, we will only consider the average first return time and define a scalar field $\tau(x,y)$ in the space of initial conditions. One can indeed assume that if near a given point (x_0,y_0) with positive $\nu(x_0,y_0)$ the average return time $\tau(x_0,y_0)$ is large, then a dye of fluid would explore a large part of phase space and so it would be best to drop the dye in its neighborhood, than in some other point with similar ν but a smaller τ .

Typically when analyzing return time statistics from a numerical perspective, one defines a small area Γ in phase

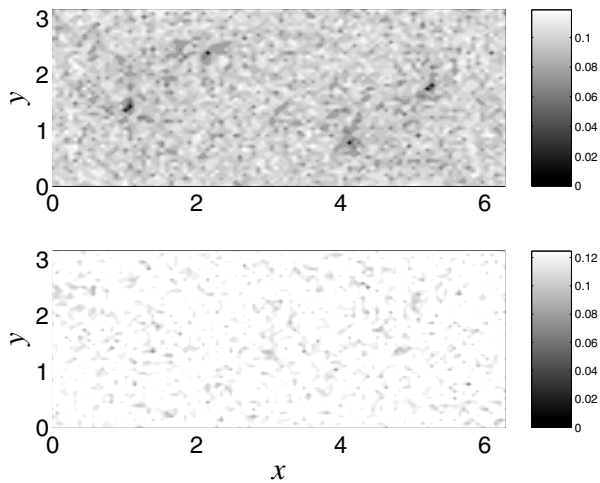


FIG. 5. Lyapunov maps for the dynamics of tracers given by the stream function Ψ_c given by Eq. (14) for $\omega=1.67$ and $\epsilon=0.63$ (upper panel) and for $\omega=1$ and $\epsilon=0.8$ (lower panel) at a time $T=200\pi$.

space and compute a distribution of return times of trajectories leaving the area. On the one side due to the fact that, for Hamiltonian systems with finite phase space, the average return time is finite and scales as $1/\Gamma$ (Kac's lemma), one must be cautious not to take Γ too small in order to carry long enough simulations and capture enough events to build a characteristic distribution. On the other hand, return time distributions are supposed to be computed for $\Gamma \rightarrow 0$. For the considered flow, due to symmetries we consider $[0, \pi] \times [0, \pi]$ as the space of initial conditions which has been divided regularly in 2500 small squares. For each square, the mean return time has been computed using two trajectories computed for 10^5 periods. Given the size of Γ , we collect for each cell about 300 events. The results are presented in logarithmic scale in Fig. 6. The parameters have been chosen identical to the ones used in Fig. 5. In contrast to the Lyapunov map, one sees that this diagnostics finds the barriers (region with long return times). For $\omega=1.67$ and $\epsilon=0.63$ (upper panel), one can also see small regions with quite low return times: They correspond to small regular islands as mentioned previously. The small return time regions have disappeared for $\omega=1$ and $\epsilon=0.8$ (lower panel).

Hence, in order to get an accurate picture of the mixing properties of the cell, one must combine the information of both the local Lyapunov exponent and the local average return time, for example, by computing the scalar field $\nu(x_0, y_0) \times \tau(x_0, y_0)$. Indeed this map shall give us information on good mixing regions, and provide as well the location of where to drop initially the dye to achieve a faster homogenization and mixing.

C. Robustness

We have identified a family of perturbations which, while keeping the cellular structure of the flow, enhance considerably mixing properties within the cells. The perturbations have been constructed for a very specific flow; hence a natu-

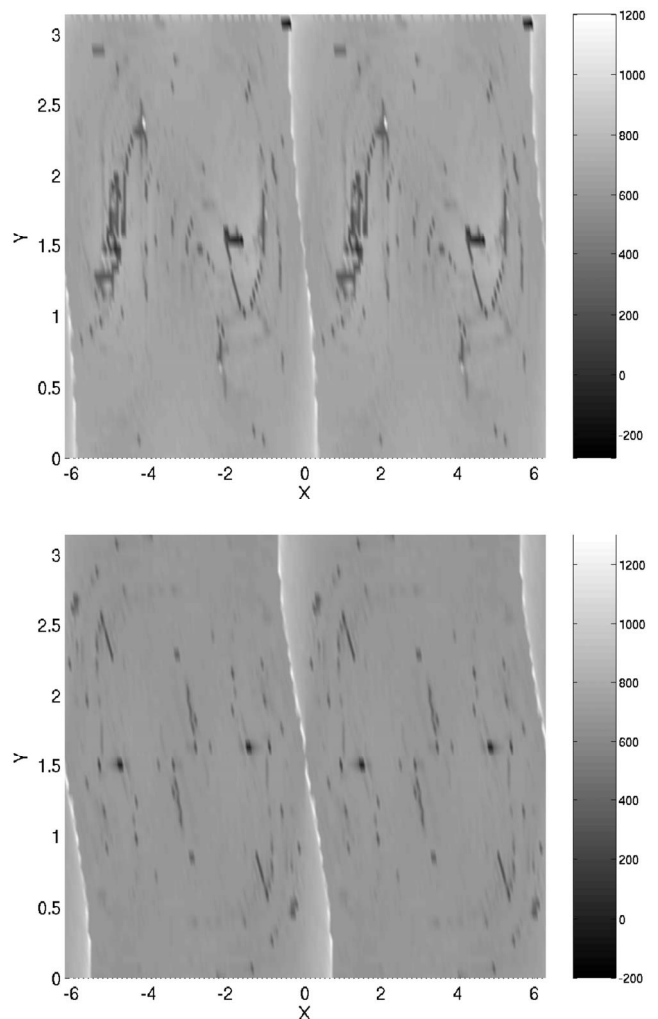


FIG. 6. Mean recurrence time in initial condition space of tracers given by the stream function Ψ_c given by Eq. (14) for $\omega=1.67$ and $\epsilon=0.63$ (upper panel) and for $\omega=1$ and $\epsilon=0.8$ (lower panel). Initial conditions space is divided into 100×50 cells. Trajectories are computed for $\sim 10^5$ periods, time steps are $dt=T/200$.

ral question arises in practical situations: Whether or not the considered perturbed system is robust with respect to small changes or errors in the applied perturbation. Indeed robustness is a key concern in order for an experimental setup using this type of perturbation. Below we analyze robustness with respect to four factors: The truncation of the time series giving the time dependence of the perturbation, the slip boundary conditions, three-dimensional effects, and molecular diffusivity.

1. Truncation of the series

From the experimental perspective we may expect some difficulties in implementing the whole series $C_\epsilon(t)$ given by Eq. (12). One may wonder how the barrier and mixing properties are affected when one truncates the series and retain for instance only the first term of the perturbation term (12), meaning only one mode is used for the perturbation, C_ϵ is replaced by $-2\mathcal{J}_1(\epsilon)\cos t$. Figure 7 represents the plot of

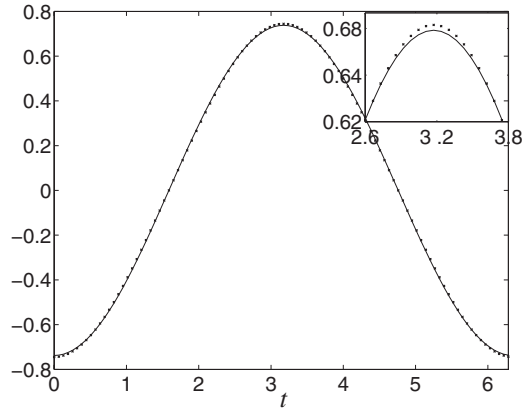


FIG. 7. Functions $C_\epsilon(t)$ (solid line) and $-2\mathcal{J}_1(\epsilon)\cos t$ (dotted line) for $t \in [0, 2\pi]$ and $\epsilon=0.8$.

these two functions for $\omega=1$ and $\epsilon=0.8$. The small discrepancy between both functions might affect significantly the transport barriers since it is well known that heteroclinic orbits are very sensitive to perturbations and are generically broken by an arbitrarily small perturbation.

Trajectories of passive particles with a dynamics given by the stream function

$$\Psi_c^{(a)}(x, y) = \sin[x + \epsilon \sin \omega t - 2\omega^{-1}\mathcal{J}_1(\epsilon)\cos \omega t \cos y] \sin y, \quad (15)$$

are displayed in Fig. 8. One can see that the barrier is leaking while mixing properties do not seem to be affected significantly. One must notice that given the time length and the amount of passive particles considered, the leak is small. The truncated series is still achieving a good “targeted mixing.”

2. No-slip boundary conditions

If one wants to take into account the thin boundary layers present on the boundaries of the channel, it amounts to consider that the fluid is confined between the two surfaces $y=0$ and $y=\pi$ with no-slip boundary conditions. In this case, the stream function is modified into

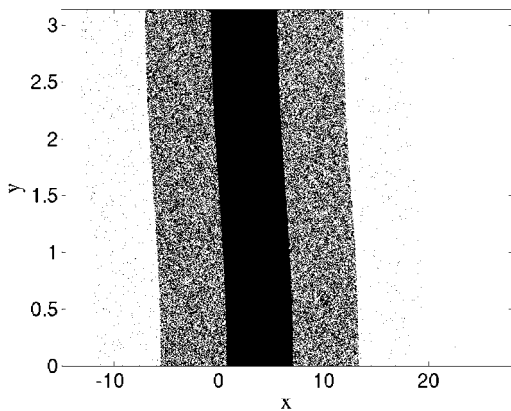


FIG. 8. Poincaré section computed with the trajectories of 1000 passive tracers and dynamics given by the stream function (15). The parameters are $\omega=1$, $\epsilon=0.8$. The integration time is 1000 periods.

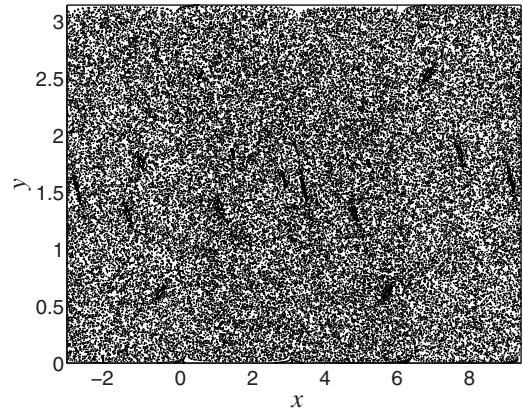


FIG. 9. Poincaré section of the perturbed stream function (18). The parameters are $\omega=1$ and $\epsilon=0.8$. The integration time is 1000 periods.

$$\Psi_0(x, y) = \sin x W(y), \quad (16)$$

where no-slip boundary conditions $\dot{x}=\dot{y}=0$ at $y=0$ and $y=\pi$ are obtained with

$$W(y) = \cos(q_0 \bar{y}) - A_1 \cosh(q_1 \bar{y}) \cos(q_2 \bar{y}) + A_2 \sinh(q_1 \bar{y}) \sin(q_2 \bar{y}), \quad (17)$$

with $\bar{y}=y/\pi-1/2$, $q_0=3.973\ 639$, $q_1=5.195\ 214$, $q_2=2.126\ 096$, $A_1=0.061\ 516\ 64$, and $A_2=0.103\ 887$ (see Ref. [45]). In this setting the resulting streamlines of the unperturbed stream function (16) are very similar to the ones in Fig. 2(a) with the difference that the velocity vanishes at the top and bottom of the channel.

In order to test the effect of the proposed perturbation (11) on the stream function (16), we consider the following perturbed stream function:

$$\Psi_c^c(x, y, t) = \sin[x + \epsilon \sin \omega t + \omega^{-1} \cos y C_\epsilon(\omega t)] W(y). \quad (18)$$

Note that the no-slip boundary conditions are maintained at $y=0$ and $y=\pi$. A Poincaré section for the stream function (18) is displayed in Fig. 9 for $\omega=1$ and $\epsilon=0.8$. The barriers are broken and we observe long-range chaotic transport of passive particles along the channel. However, the mixing properties are maintained in the major part of the channel, except for some areas where some very small regular regions remain.

Nevertheless, the exact perturbation of the stream function (16) can be derived following the method developed in Sec. II A. It gives the following stream function:

$$\Psi_c(x, y, t) = \sin[x + \epsilon \sin \omega t + \omega^{-1} W'(y) C_\epsilon(\omega t)] W(y), \quad (19)$$

which preserves the no-slip boundary conditions at $y=0$ and $y=\pi$. The resulting Poincaré section depicted on Fig. 10, for $\omega=1$ and $\epsilon=0.8$, shows, as in the case of Fig. 3(b), that the stream function (19) keeps the transport barriers and the mixing properties.

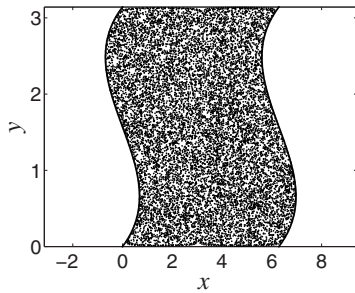


FIG. 10. Poincaré section of the stream function (19). The parameters are $\omega=1$ and $\epsilon=0.8$.

3. Three-dimensional effects

If the flow is bounded, depending on the size of the boundary layers and the fluid extension in the third direction, nonuniform vorticity can give rise to a secondary instability leading to a three-dimensional flow (Ekman pumping). Hence, for the considered perturbed flow, we may need to take into account the weakly three-dimensional case, which may be given by the empirical flow (see, for instance, [46])

$$\begin{aligned}\dot{x} &= -\sin x \cos y + \epsilon_1 \sin 2x \sin z, \\ \dot{y} &= \cos x \sin y + \epsilon_1 \sin 2y \sin z, \\ \dot{z} &= 2\epsilon_1 \cos z (\cos 2x + \cos 2y).\end{aligned}\quad (20)$$

Note that the strength of the third component of the flow is characterized by ϵ_1 .

In order to study how well the two-dimensional barrier fares in this three-dimensional flow, we apply the perturbation given by Eq. (11) to the right-hand side of Eq. (20). The perturbed system is then given by

$$\begin{aligned}\dot{x}_s &= -\sin x_s \cos y + \epsilon_1 \sin 2x_s \sin z + \omega^{-1} C_\epsilon(\omega t) \cos x_s \sin^2 y, \\ \dot{y} &= \cos x_s \sin y + \epsilon_1 \sin 2y \sin z, \\ \dot{z} &= 2\epsilon_1 \cos z (\cos 2x_s + \cos 2y),\end{aligned}\quad (21)$$

where $x_s = x + \epsilon \sin \omega t + \omega^{-1} \cos y C_\epsilon(\omega t)$. We notice that an additional term has been added to \dot{x} in order to ensure a divergence free field.

Keeping a two-dimensional point of view of the system (21), we visualize the projections in the (x, y) plane of the position of passive tracers. When considering $\epsilon_1=0.005$ and 4×10^4 passive particles at time $t=10T$, where $T=2\pi$, an effective barrier remains as it is shown in Fig. 11(a) and mixing properties are not affected, but we observe some advected particles which escape from the cell. However as depicted in Fig. 11(b), when the integration time is $t=100T$ (for the same value of ϵ_1 and number of particles), the barrier still influences the motion but leaks since a more significant number of particles get through these barriers.

4. Molecular diffusivity

Finally, we have up to now considered ideal passive tracers, which are not subject to any molecular diffusivity, which

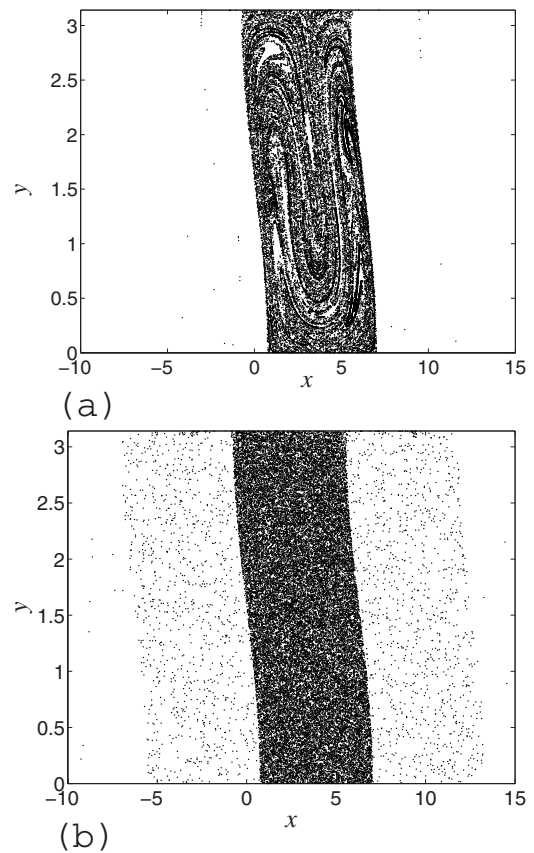


FIG. 11. Projection of trajectories of the system (20) for $\omega=1$, $\epsilon=0.8$, and $\epsilon_1=0.005$. (a) $t=10T$; (b) $t=100T$.

may be a good approximation for high Peclet numbers. However, it is likely that for any finite molecular diffusivity the barrier will leak. In order to illustrate this phenomenon, we consider that tracers are actually subject to a Langevin equation associated with the stream function Ψ_c given by Eq. (14),

$$\dot{x} = -\frac{\partial \Psi_c}{\partial y} + b_x(t), \quad \dot{y} = \frac{\partial \Psi_c}{\partial x} + b_y(t), \quad (22)$$

where $b_x(t)$ and $b_y(t)$ are two independent δ -correlated white noises, with zero mean and a given amplitude μ . Numerical results are displayed in Fig. 12, where $\mu=4 \times 10^{-2}$ (which corresponds to Peclet number of $Pe \approx 600$), $\omega=1$, and $\epsilon=0.8$. In order to avoid crossing across the “walls” $y=\pi$ and $y=0$, we took $b_y=0$.

One can see that for this type of Peclet values, the transport barrier is indeed leaking, and in fact the truncation of $C_\epsilon(t)$ does not affect how much the barrier leaks.

In summary the robustness of the proposed perturbation in different settings has been investigated. One may infer that the most drastic effects are induced by boundary conditions. On the other hand, provided that the correct perturbation is computed, one concludes that if three-dimensional effects are weak and Peclet number is high enough, a truncation to the first term of the series $C_\epsilon(t)$ is sufficient, and actually implementing more terms seems useless.

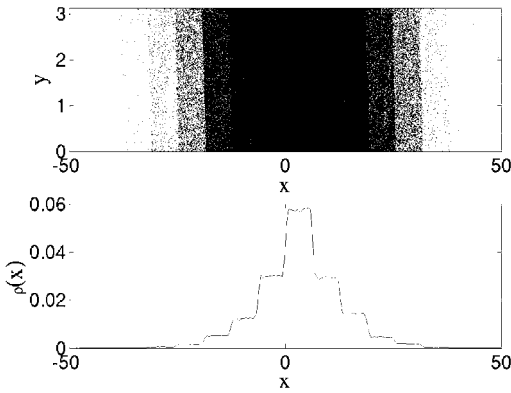


FIG. 12. Trajectories of 1000 passive tracers given by Eq. (22). (Top) Local density of tracers. (Bottom) The parameters are $\mu=4 \times 10^{-2}$ (Peclet number $Pe \approx 600$), $\omega=1$ and $\epsilon=0.8$. The integration time is 1000 periods.

D. Targeted mixing regimes

It was shown in Sec. II A that a perturbation allows one to localize tracers into a finite volume of phase space. However, depending on the values of the parameters of the perturbation (ω, ϵ) in Eq. (14), some regular islands may exist and prevent complete mixing inside the cell. In this section we propose to identify the domain of parameters (if any) such that these islands do not exist and the cell become fully mixing.

This domain in parameter space can be determined by analyzing the linear stability of a few periodic orbits of the system as discussed in Sec. II B. These orbits are those with low rotation numbers, around which the resonant islands organize. Indeed, an island is organized around a central elliptic orbit: If the latter were to turn hyperbolic, the dynamics might become (locally) chaotic, since generically chaos is expected in the neighborhood of hyperbolic orbits by an infinite number of intersections between its stable and unstable manifolds. In order to monitor these orbits, we use a scalar indicator of linear stability, such as the residue (see Sec. II B). The fully mixing regime will then correspond to the residues of selected periodic orbits being below 0 or above 1. However, the change of linear stability of a given periodic orbit might not change its nonlinear stability and still preserve invariant tori in its neighborhood. This linear stability analysis of periodic orbits must be completed by an *a posteriori* check to determine whether or not the regular island has disappeared with the elliptic periodic orbit turning hyperbolic.

Let us consider the following range of parameters $(\omega, \epsilon) \in [0.6, 2.2] \times [0, 2.2]$. Inspection of several Poincaré sections reveals that in this range, it is essentially the nature of eight periodic orbits which drives the mixing properties inside the cell. However, thanks to the symmetry with respect to the point $(x, y) = (\pi, \pi/2)$, this set reduces to only four orbits: Three of them have rotation number one, namely O_1 , O_1^α and O_1^β , while the fourth one, called O_2^+ has a rotation number $Q=2$. Depending on the value of the parameters (ω, ϵ) , these orbits can be elliptic—and create resonant islands around them—or hyperbolic. In order to describe the

nature of each of these four orbits for a given value of parameters, we use the nomenclature $[N(O_1)N(O_2^+)N(O_1^\alpha)N(O_1^\beta)]$, with $N(O)=h$ if O is hyperbolic, e if elliptic, and 0 if it does not exist. Let us precise that there also exists a hyperbolic orbit with $Q=2$, called O_2^- , which forms a Birkhoff pair with O_2^+ . As it remains hyperbolic in the range of parameters under consideration, it only provides a better understanding of the bifurcation process, but does not influence the mixing properties inside the cell.

Figure 13 depicts Poincaré sections for eight different values of parameters. These cases illustrate some possible mixing regimes in the considered range of parameters. Figures 13(a)–13(d) (corresponding, respectively, to $[hh00]$, $[he00]$, $[eh00]$, and $[ee00]$) show how O_1 and O_2^+ can coexist in their two forms (elliptic and hyperbolic), the full mixing regime being reached when both are hyperbolic as in Fig. 13(a) where it is $[hh00]$. We notice that when O_1 or O_2^+ is elliptic, the mixing is only prevented by the elliptic island. Only small secondary islands are observed [for instance, in Fig. 13(c)]. This reinforces the importance of the considered set of periodic orbits for mixing properties.

For smaller values of ω , the orbits O_1^α and O_1^β may also appear (if $\omega \leq 1.2$ and large ϵ for O_1^α , or $\omega \leq 1$ and small ϵ for O_1^β), and their nature must be taken into account, as one can see in Fig. 13(e) $[hhe0]$, where the hyperbolicity of O_1 and O_2^+ is not sufficient to ensure the full mixing inside the cell, as O_1^α is present in its elliptic form. Mixing can still be obtained in the presence of O_1^β , as can be seen in Fig. 13(f) which corresponds to the case $[hh0h]$. The opposite case $[ee0e]$ is depicted in Fig. 13(h) where all three orbits are elliptic and almost no mixing occurs.

Finally, one can see in Fig. 13 which is $[e000]$ how for large values of ω (typically beyond 2), O_2^+ no longer exists, while O_1 stays elliptic: Furthermore, new resonant islands have appeared, associated with new periodic orbits (with $Q=3$ and $Q=5$ as shown). This illustrates the fact that in another range of parameters, the dynamics may be guided by higher order periodic orbits which are associated with smaller islands.

A better insight in the bifurcation scheme can be gained by varying only one parameter at a time. Figure 14 depicts the residue curves associated with the orbits O_1 , O_2^+ , O_2^- , O_1^α , and O_1^β when varying ϵ and keeping ω constant. Two curves have been computed in the intermediate frequency range $\omega=1.42$ and $\omega=1.67$. In the intermediate regime, only three of these five orbits exist, namely O_1 (plain line), O_2^+ and O_2^- (respectively, upper and lower dashed-dotted lines).

For $\omega=1.42$ [see Fig. 14(a)] and for low ϵ , both O_1 and O_2^+ are elliptic: only partial mixing occurs. While O_2^+ turns hyperbolic as ϵ is increased (around $\epsilon \approx 0.2$), O_1 remains elliptic until $\epsilon \approx 0.4$. O_1 turns from elliptic to hyperbolic by merging with O_2^- , according to the process

$$O_2^-[h] + O_1[e] \rightarrow O_1[h]. \quad (23)$$

This bifurcation does not happen just for this particular choice of parameters, but appears to be fairly generic in this range of parameters. For a better illustration of this process, the behavior of the eigenvalues of the monodromy matrix

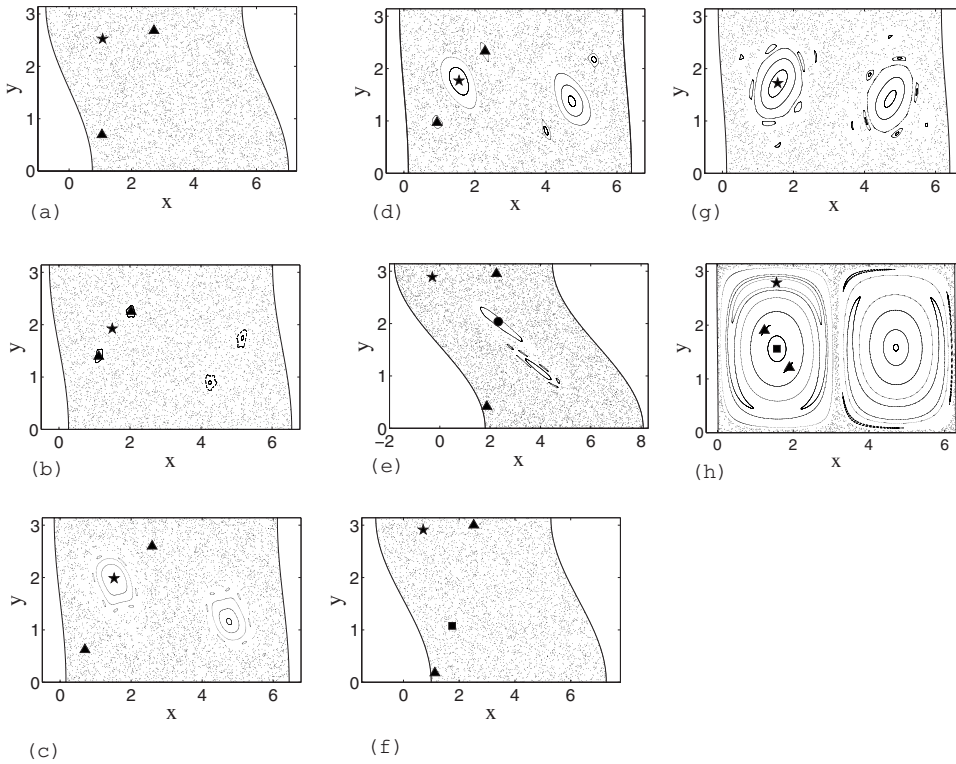


FIG. 13. Poincaré sections in the different domains of parameters (ω, ϵ) for the stream function (14). The stars, full circles, squares, and triangles indicate, respectively, the locations of O_1 , O_1^α , O_1^β , and O_2^+ . (a) $\omega=1, \epsilon=0.8$; (b) $\omega=1.8, \epsilon=0.5$; (c) $\omega=1.2, \epsilon=0.2$; (d) $\omega=1.6, \epsilon=0.2$; (e) $\omega=0.58, \epsilon=1.25$; (f) $\omega=0.58, \epsilon=0.6$; (g) $\omega=2.1, \epsilon=0.25$; (h) $\omega=0.63, \epsilon=0.01$.

associated with O_1 in shown in Fig. 15 (for $\omega=1.67$, similar to the case $\omega=1.42$). The two eigenvalues, initially conjugated on the unity circle (i.e., O_1 is elliptic), encounter a period doubling bifurcation when they reach 1, and leave the unity circle: O_1 has turned hyperbolic. Then they are of the form $(\lambda, 1/\lambda), \lambda \in \mathbb{R}^*$. Eventually, the phenomenon will revert, the eigenvalues going back on the circle and O_1 to ellipticity. For ϵ between 0.4 and 0.9, the orbits O_1 , O_2^+ , and O_2^- are all hyperbolic, acknowledging a complete mixing. Then, increasing further ϵ , the orbit O_2^+ turns elliptic after $\epsilon \approx 0.9$, and hence mixing decreases. It remains so until it merges with the hyperbolic O_1 , at $\epsilon \approx 1.1$, to give an elliptic O_1 (parabolic at the transition), according to the scheme

$$O_2^+[e] + O_1[h] \rightarrow O_1[e]. \quad (24)$$

Beyond $\epsilon \approx 1.4$, the only remaining orbit, O_1 , stays elliptic.

For $\omega=1.67$ [see Fig. 14(b)], the dynamics is more regular: While bifurcation (23) still occurs, resulting in a hyperbolic O_1 , the residue of O_2^+ never crosses 1, which means that the orbit stays elliptic. Around $\epsilon \approx 0.9$, it merges with the hyperbolic O_1 to give an elliptic O_1 , according to the bifurcation (24). Beyond this point, O_1 will stay elliptic: Full mixing cannot be achieved for such values of ω .

Three other curves illustrate the behaviors at low frequency, i.e., $\omega=0.8$ and $\omega=0.58$, and at a high frequency $\omega=2.08$.

For $\omega=0.8$ [see Fig. 14(c)], the bifurcation scheme is more complicated due to the presence of the orbit O_1^α and O_1^β (respectively right and left dashed line). The orbits can either exist in an elliptic or hyperbolic way, or not exist at all. The two latter cases, combined with O_1 and O_2^+ hyperbolicity, are suitable for a fully mixing regime.

For low ϵ , though O_2^+ turns hyperbolic very soon (at $\epsilon \approx 0.05$), O_1^β is elliptic until $\epsilon \approx 0.2$, when it disappears. However, because of the ellipticity of O_1 , full mixing cannot occur until it also turns hyperbolic, at $\epsilon \approx 0.3$. Then complete mixing is achieved until $\epsilon \approx 1.5$, when O_2^+ turns back elliptic, soon followed by O_1 when they merge according to the bifurcation scheme (24). Note that around $\epsilon \approx 1.6$, orbit O_1^α appears, but full mixing is no longer possible because of O_1 ellipticity.

Then, for $\omega=0.58$, the bifurcation scheme is more intricate due to the fact that O_1^β turns hyperbolic. For low ϵ , despite O_2^+ and O_1 soon turn hyperbolic (at $\epsilon \approx 0.2$ for the latter), O_1^β remains elliptic until $\epsilon \approx 0.5$, when its residues go above 1: Full mixing is then achieved [see Fig. 13(f)], until the orbit returns to ellipticity at $\epsilon \approx 0.65$. However, it disappears at $\epsilon \approx 0.7$, and then only O_1 and O_2^+ are present, in their hyperbolic form; thus mixing is achieved anew. It remains so until $\epsilon \approx 1.1$, when O_1^α comes into play, being elliptic. Furthermore, it will also be hyperbolic (around $\epsilon \approx 2$), but only when O_1 has turned back to ellipticity: Mixing will not occur any longer.

For large ω [$\omega=2.08$, see Fig. 14(e)], the dynamics is more regular. The orbits O_2^+ and O_2^- do not exist, and the only remaining orbit, O_1 , never encounters any bifurcation, and stays elliptic. Complete mixing cannot be achieved in this case either.

Now, instead of varying the amplitude ϵ of the forcing, we vary its frequency ω and keep ϵ constant. For $\epsilon=0.8$ [see Fig. 16(a)] and for ω below 0.55, the orbit O_1^β is hyperbolic as well as O_1 and O_2^+ : The cell is fully mixing. Soon after O_1^β turns elliptic at $\omega \approx 0.55$, it disappears around $\omega \approx 0.57$; the remaining orbits are hyperbolic until O_2^+ turns elliptic ($\omega \approx 1.55$). Finally, at $\omega \approx 1.8$, the elliptic O_2^+ merges with the

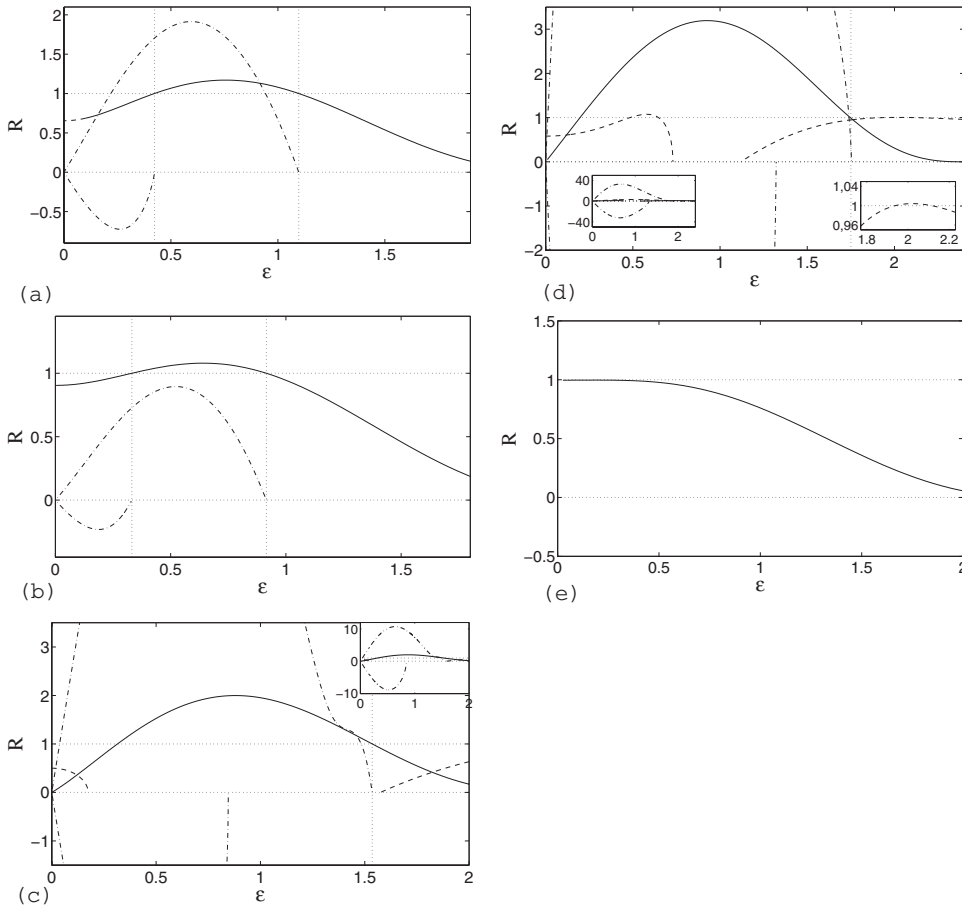


FIG. 14. Residue curves for the stream function (14) as functions of the amplitude ϵ : The plain line corresponds to the residues of O_1 , the dashed line corresponds to the residues of O_1^β , and the dashed-dotted line corresponds to the ones of O_2^+ (upper curve) and O_2^- (lower curve). The dotted line indicates the locations of the bifurcations. (a) $\omega=1.42$; (b) $\omega=1.67$; (c) $\omega=0.8$; (d) $\omega=0.58$; (e) $\omega=2.08$.

hyperbolic O_1 [as described by the bifurcation (24)] to give an elliptic O_1 : Only partial mixing is achieved.

For $\epsilon=0.4$ [see Fig. 16(b)], the situation is slightly different: For low ω , the orbit O_1^β (plain line) is present and mostly elliptic. Its residue is higher than 1 only in a small range of ω [around $\omega=0.61$, see the inset of Fig. 16(b)], and only this small domain of ω is suitable for complete mixing, since O_1 and O_2^+ are hyperbolic for small ω . Then, for $\omega \approx 0.7$, the elliptic O_1^β disappears, and as long as O_1 (dashed line) and O_2^+ (dashed-dotted line) are hyperbolic, the cell is still fully mixing. Around $\omega=1$, O_1 turns elliptic and so mixing is only partial. Moreover, when it turns back to hyperbolicity for $\omega \approx 1.55$, the orbit O_2^+ soon becomes elliptic: The parameter range available for complete mixing is small. Finally, O_2^+ merges with the hyperbolic O_1 through the bifurcation (24), leaving an elliptic O_1 : Full mixing cannot be achieved any more.

Figure 17 summarizes the residue study with the domain of ellipticity and/or hyperbolicity of these orbits. The domains of parameters are noted with letters, in agreement with the labeling of Fig. 13. The gray colored domain is the most suitable for complete mixing, since O_1 and O_2^+ are hyperbolic, while O_1^β and O_1^α do not exist. The domain (f) would also be suitable; however, in this range of parameters, new orbits are born when ϵ decreases.

IV. CONCLUSION AND PERSPECTIVES

Time-periodic perturbations are able to generate chaotic mixing in two-dimensional channels. Optimal mixing is ob-

tained when all regular structures are broken by the perturbation. We have shown here that this optimal mixing can be obtained in a small domain of phase space by combining two strategies: First, by constructing two transport barriers, confining the fluid in a bounded region of the channel. Generically, it is expected that the motion inside this bounded cell is a mixture of regular (nonmixing) regions and chaotic (mixing) ones. Then, using the linear stability of a few selected periodic orbits (represented by their residues) and the identification of bifurcations, we gave conditions on the parameters of the system (represented by the amplitude and the frequency of the periodic forcing) such that a high mixing occurs in the cell. We have shown that complete mixing is expected in a large region of parameter space. The mixing properties have been *a posteriori* analyzed and confirmed by computing a finite time Lyapunov map of initial conditions

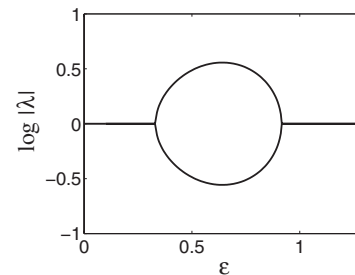


FIG. 15. Modulus of the eigenvalues of orbit O_1 for the stream function (14) with $\omega=1.67$.

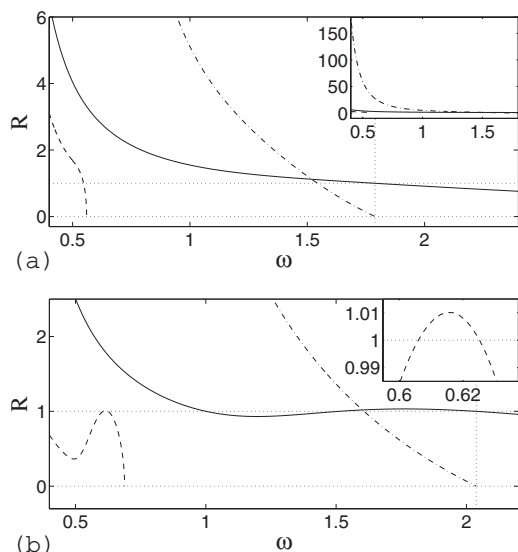


FIG. 16. Residue curves for the stream function (14) as functions of the frequency ω : The plain line corresponds to the residues of O_1 , the dashed line corresponds to the residues of O_1^β , and the dashed-dotted line corresponds to the ones of O_2^+ (upper curve) and O_2^- (lower curve). The dotted lines indicate the locations of the bifurcations. (a) $\epsilon=1.42$; (b) $\epsilon=0.4$.

space. Moreover, a strategy for placing an initial drop of dye has been proposed by combining the information of the finite time Lyapunov map with a map in initial conditions space of average return times. Finally, we have shown that the strategy we developed is robust to several effects like truncations of the Fourier series giving the exact shape of the perturba-

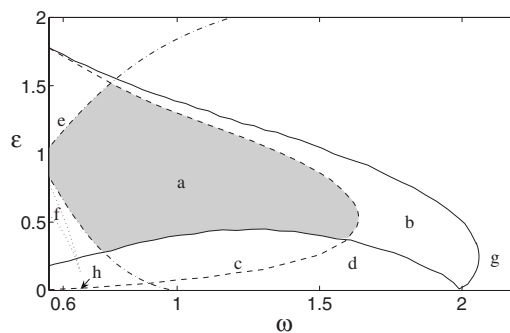


FIG. 17. Mixing domains for the stream function (14) in parameter space: The letters (a)–(h) refer to mixing regimes as depicted in the typical Poincaré sections in Fig. 13. The gray domain represents the expected mixing regime where the studied periodic orbits are all hyperbolic (or non-existent). The plain curve is associated with the orbit O_1 where its residue is equal to 1; the dashed curve is associated with the orbit O_2^+ ; the upper dashed-dotted line bounds the domain of existence of O_1^α (it is elliptic above and does not exist below), while the lower dashed-dotted line delimits the one of O_1^β (existing below but not above). While the latter orbit is mainly elliptic, the dotted line encloses the small domain where it is hyperbolic.

tion, three-dimensional effects, and molecular diffusion. When no-slip boundary conditions apply, it must be taken into account in the computation of the perturbation since the restored transport barriers are not robust without this, although the good mixing properties do not seem to be affected.

-
- [1] H. Aref, *J. Fluid Mech.* **143**, 1 (1984).
 [2] H. Aref, *Philos. Trans. R. Soc. London, Ser. A* **333**, 273 (1990).
 [3] J. Ottino, *The Kinematics of Mixing: Stretching, Chaos, and Transport* (Cambridge University Press, Cambridge, 1989).
 [4] J. Ottino, *Annu. Rev. Fluid Mech.* **22**, 207 (1990).
 [5] G. M. Zaslavsky, R. Z. Sagdeev, D. A. Usikov, and A. A. Chernikov, *Weak Chaos and Quasiregular Patterns* (Cambridge University Press, Cambridge, 1991).
 [6] A. Crisanti, M. Falcioni, G. Paladin, and A. Vulpiani, *Riv. Nuovo Cimento* **14**, 1 (1991).
 [7] A. B. Rechester and R. B. White, *Phys. Rev. Lett.* **44**, 1586 (1980).
 [8] T. H. Solomon, E. R. Weeks, and H. L. Swinney, *Physica D* **76**, 70 (1994).
 [9] X. Leoncini, O. Agullo, S. Benkadda, and G. M. Zaslavsky, *Phys. Rev. E* **72**, 026218 (2005).
 [10] G. M. Zaslavsky, *Phys. Rep.* **371**, 641 (2002).
 [11] M. G. Brown and K. B. Smith, *Phys. Fluids A* **3**, 1186 (1991).
 [12] R. Behringer, S. Meyers, and H. Swinney, *Phys. Fluids A* **3**, 1243 (1991).
 [13] A. A. Chernikov, B. A. Petrovichev, A. V. Rogal'sky, R. Z. Sagdeev, and G. M. Zaslavsky, *Phys. Lett. A* **144**, 127 (1990).
 [14] F. Dupont, R. I. McLachlan, and V. Zeitlin, *Phys. Fluids* **10**, 3185 (1998).
 [15] A. Crisanti, M. Falcioni, A. Provenzale, P. Tanga, and A. Vulpiani, *Phys. Fluids A* **4**, 1805 (1992).
 [16] B. A. Carreras, V. E. Lynch, L. Garcia, M. Edelman, and G. M. Zaslavsky, *Chaos* **13**, 1175 (2003).
 [17] S. V. Annibaldi, G. Manfredi, R. O. Dendy, and L. O. Drury, *Plasma Phys. Controlled Fusion* **42**, L13 (2000).
 [18] D. del Castillo-Negrete, B. A. Carreras, and V. E. Lynch, *Phys. Plasmas* **11**, 3854 (2004).
 [19] S. Balasuriya, *Physica D* **202**, 155 (2005).
 [20] A. Stroock, S. Dertinger, A. Ajdari, I. Mezic, H. Stone, and G. Whitesides, *Science* **295**, 647 (2002).
 [21] T. H. Solomon and J. P. Gollub, *Phys. Rev. A* **38**, 6280 (1988).
 [22] T. Solomon, N. Miller, C. Spohn, and J. Moeur, *AIP Conf. Proc.* **676**, 195 (2003).
 [23] H. Willaime, O. Cardoso, and P. Tabeling, *Phys. Rev. E* **48**, 288 (1993).
 [24] R. Camassa and S. Wiggins, *Phys. Rev. A* **43**, 774 (1991).
 [25] L. Kuznetsov and G. M. Zaslavsky, *Phys. Rev. E* **61**, 3777 (2000).
 [26] X. Leoncini, L. Kuznetsov, and G. M. Zaslavsky, *Phys. Rev. E* **63**, 036224 (2001).
 [27] D. L. Vainchtein, J. Widloski, and R. O. Grigoriev, *Phys. Fluids* **19**, 067102 (2007).

- [28] E. Villermaux and J. Duplat, *Phys. Rev. Lett.* **91**, 184501 (2003).
- [29] P. Castiglione, A. Mazzino, P. Mutatore-Ginanneschi, and A. Vulpiani, *Physica D* **134**, 75 (1999).
- [30] M. S. Paoletti, C. R. Nugent, and T. H. Solomon, *Phys. Rev. Lett.* **96**, 124101 (2006).
- [31] C. Chandre, G. Ciraolo, F. Doveil, R. Lima, A. Macor, and M. Vittot, *Phys. Rev. Lett.* **94**, 074101 (2005).
- [32] R. Bachelard, C. Chandre, and X. Leoncini, *Chaos* **16**, 023104 (2006).
- [33] T. Benzekri, C. Chandre, X. Leoncini, R. Lima, and M. Vittot, *Phys. Rev. Lett.* **96**, 124503 (2006).
- [34] M. Cencini, A. Torcini, D. Vergni, and A. Vulpiani, *Phys. Fluids* **15**, 679 (2003).
- [35] M. S. Paoletti and T. H. Solomon, *Europhys. Lett.* **69**, 819 (2005).
- [36] M. S. Paoletti and T. H. Solomon, *Phys. Rev. E* **72**, 046204 (2005).
- [37] S. Berti, D. Vergni, F. Visconti, and A. Vulpiani, *Phys. Rev. E* **72**, 036302 (2005).
- [38] A. Pocheau and F. Harambat, *Phys. Rev. E* **73**, 065304(R) (2006).
- [39] P. Cvitanović, R. Artuso, R. Mainieri, G. Tanner, and G. Vattay, *Chaos: Classical and Quantum* (Niels Bohr Institute, Copenhagen, 2005).
- [40] R. S. MacKay, *Nonlinearity* **5**, 161 (1992).
- [41] J. M. Greene, *Phys. Fluids* **20**, 1183 (1979).
- [42] J. R. Cary and J. D. Hanson, *Phys. Fluids* **29**, 2464 (1986).
- [43] S. Wiggins, *Chaotic Transport In Dynamical Systems* (Springer-Verlag, Berlin, 1992).
- [44] N. Haydn, E. Lunedei, L. Rossi, G. Turchetti, and S. Vaienti, *Chaos* **15**, 033109 (2005).
- [45] S. Chandrasekhar, *Hydrodynamics and Hydrodynamic Stability* (Dover, New York, 1961).
- [46] T. Solomon and I. Mezic, *Nature (London)* **425**, 376 (2003).